Optimal Coordinated Transmit Beamforming for Networked Integrated Sensing and Communications

Gaoyuan Cheng, Yuan Fang, Jie Xu, and Derrick Wing Kwan Ng

Abstract—This paper studies a multi-antenna networked integrated sensing and communications (ISAC) system, in which a set of multi-antenna base stations (BSs) employ the coordinated transmit beamforming to serve multiple single-antenna communication users (CUs) and perform joint target detection by exploiting the reflected signals simultaneously. To facilitate target sensing, the BSs transmit dedicated sensing signals combined with their information signals. Accordingly, we consider two types of CU receivers with and without the capability of canceling the interference from the dedicated sensing signals, respectively. In addition, we investigate two scenarios with and without time synchronization among the BSs. For the scenario with synchronization, the BSs can exploit the target-reflected signals over both the direct links (BS-to-target-to-originated BS links) and the cross-links (BS-to-target-to-other BSs links) for joint detection, while in the unsynchronized scenario, the BSs can only utilize the target-reflected signals over the direct links. For each scenario under different types of CU receivers, we optimize the coordinated transmit beamforming at the BSs to maximize the minimum detection probability over a particular targeted area, while guaranteeing the required minimum signal-to-interference-plus-noise ratio (SINR) constraints at the CUs. These SINR-constrained detection probability maximization problems are recast as non-convex quadratically constrained quadratic programs (QCQPs), which are then optimally solved via the semi-definite relaxation (SDR) technique. The numerical results show that for each considered scenario, the proposed ISAC design achieves enhanced target detection probability compared with various benchmark schemes. In particular, enabling time synchronization and sensing signal cancellation at the BSs is always beneficial for further improving the joint detection and communication performance.

Index Terms—Networked integrated sensing and communications (ISAC), coordinated transmit beamforming, target detection, semi-definite relaxation, likelihood ratio test.

I. INTRODUCTION

INTEGRATED sensing and communications (ISAC) has been recognized as one of the usage scenarios of sixth-generation (6G) wireless networks [2]–[6] to support emerging applications such as auto-driving, smart city, industrial automation, and unmanned aerial vehicles (UAVs) [7]–[9]. Specifically, ISAC allows the sharing of cellular base station (BS) infrastructures, signal processing modules, as well as

G. Cheng, Y. Fang, and J. Xu are with the School of Science and Engineering (SSE), Future Network of Intelligence Institute (FNii), The Chinese University of Hong Kong (Shenzhen), Shenzhen 518172, China (e-mail: gaoyuancheng@link.cuhk.edu.cn, fangyuan@cuhk.edu.cn, xujie@cuhk.edu.cn). J. Xu is the corresponding author.

D. W. K. Ng is with the School of Electrical Engineering and Telecommunications, University of New South Wales, Sydney, NSW 2052, Australia (e-mail: w.k.ng@unsw.edu.au).

scarce spectrum and power resources for the dual roles of wireless communications and radar sensing. This not only enhances the utilization efficiency of limited resources, but also enables seamless coordination and mutual assistance between communication and sensing for improving their performances with reduced costs. In particular, by enabling the joint optimization of the sensing and communication transmit waveforms, beamforming, and resource allocation, ISAC can efficiently harness the co-channel interference and provide new design degrees of freedom for enhancing system performance.

Conventionally, mono-static and bi-static ISAC systems have been widely investigated in the literature (see, e.g., [10]–[21] and the references therein), in which one BS serves as an ISAC transceiver or two BSs operate as the ISAC transmitter and the sensing receiver, respectively. For instance, the authors in [16], [19] considered the transmit beamforming in a downlink ISAC system, where a BS sends combined information-bearing and dedicated sensing signals to perform downlink multiuser communication and radar target sensing simultaneously. In particular, two joint beamforming designs were investigated in [16], one aimed to match the transmit beampattern with a desired one and the other aimed to maximize the transmit beampattern gains towards desired target directions, while ensuring the communication quality of service (QoS) requirements. Also, the mean square error of the beampattern as well as the cross correlation pattern were optimized in [19] to enhance the performance of multiple-input multiple-output (MIMO) radar, subject to the communication QoS constraints. Moreover, a multi-antenna ISAC system adopting rate splitting multiple access (RSMA) was studied in [21], in which the joint transmission of communication streams and radar sequences was jointly optimized for optimizing the ISAC performance. However, the mono-static and bi-static ISAC systems can only offer limited service coverage and the resulting sensing and communication performances may degrade when there are rich obstacles in the environment and/or when the communication users (CUs) and sensing targets are located far apart from the BS.

Recently, motivated by multi-BS cooperation for communications (e.g., coordinated multi-point transmission/reception [22], [23], cloud-radio access networks (C-RAN) [24], cell-free MIMO [25], etc.) and distributed MIMO radar sensing [26]–[30], the notions of networked ISAC [31]–[33] or perceptive mobile networks [34]–[37] have drawn significant research momentum to address the aforementioned issues. On the one hand, as compared with conventional cellular architectures, C-RAN and cell-free MIMO allow centralized signal processing at the cloud to enable cooperative transmission and reception

among distributed BSs, thus effectively mitigating or even exploiting the interference originating from different CUs to enhance their communication performance [22], [24], [25]. On the other hand, a distributed MIMO radar is able to exploit the inherent spatial diversity of target radar cross section (RCS) by designing orthogonal waveforms, thus enhancing both the sensing accuracy in estimating target parameters and the detection probability [29], [38]. Besides, the coherent processing in MIMO radar can be further adopted to acquire high-resolution target detection exploiting both time and phase synchronization among different radar transceivers [39]. As such, by unifying the BSs' cooperative communications and distributed MIMO radar in integrated systems, networked ISAC is envisioned to provide seamless sensing and communication coverage, efficient interference management, enhanced communication data rate, high-resolution and high-accuracy detection and estimation [40], as well as reduced energy and hardware costs.

In the literature, there have been a handful of prior works, e.g., [31]–[33], studying networked ISAC. For instance, the authors in [31] studied a single-antenna networked ISAC system, in which different BSs jointly optimized their transmit power control to minimize the total transmit power consumption, while fulfilling the required individual signal-to-interference-plus-noise ratio (SINR) constraints set by the associated CUs and the estimation accuracy or Cramér-Rao bound (CRB) constraint for localizing a target. In addition, the work [32] considered cell-free massive MIMO for networked ISAC with regularized zero-forcing (ZF) transmit beamforming, in which the BSs jointly optimized their transmit power control over different CUs to maximize the sensing signal-to-noise ratio (SNR) while ensuring the minimum required communication SINR at the CUs. Furthermore, the work [33] investigated the network utility maximization problem for a multi-UAV networked ISAC system, in which multiple UAVs serve a group of CUs and cooperatively sense the target simultaneously. Despite the research progress on networked ISAC, however, these prior works only considered the design of transmit power control at single-antenna BSs [31], [33] or employed the simplified regularized ZF transmit beamforming at multi-antenna BSs [32]. Furthermore, these works only reused the information signals for performing target sensing [31], [33] or employing only one additional common dedicated sensing beam for facilitating the target detection at a known location [32]. To the best of our knowledge, the joint optimization of transmit information beamforming and general-rank transmit sensing beamforming in multi-antenna networked ISAC systems has not been well investigated in the literature yet. This task, however, is particularly challenging due to the following reasons. First, while the information and sensing signals at multiple BSs may cause interference at different CUs, these signals can also be jointly exploited for performing target sensing. As a result, this introduces a new tradeoff between mitigating the co-channel interference to enhance the communication performance and increasing the sensing signal strength to improve the sensing performance. Next, practical dedicated sensing signals can be generated offline and are known to each CU prior to transmission [16]. Therefore, this

presents a new opportunity to exploit interference cancellation to enhance the SINR at the CUs. However, the impact of such interference cancellation on the networked ISAC has not been investigated thus far. Furthermore, distributed MIMO sensing may exploit the cross-link echo signals from one sensing transmitter to a target captured by another sensing receiver for facilitating sensing [29], when perfect synchronization can be achieved between them. Indeed, investigating the impact of such synchronization in the performance of networked ISAC is an intriguing problem that remains unexplored. To address the above issues, the joint design of target detection and multiuser communication in networked ISAC are of utmost importance.

This paper studies a multi-antenna networked ISAC system, in which a set of multi-antenna BSs employ coordinated transmit beamforming to serve their associated CUs and at the same time reuse the reflected wireless signals to perform joint target detection. Our main results are summarized as follows.

- To fully utilize the degrees of freedom for sensing, the BSs sends dedicated sensing signals in addition to communication signals. Accordingly, to exploit the benefit of these newly introduced dedicated sensing signals, we consider two types of CU receivers: those without the capability of canceling the interference from dedicated sensing signals (Type-I receivers) and those with the capability to perform that (Type-II receivers), respectively.
- We consider two target detection scenarios depending on the availability of time synchronization among the BSs. In Scenario I, these BSs are all synchronized in time such that they can exploit the target-reflected signals over both the direct links (BS-to-target-to-originated BS links) and the cross links (BS-to-target-to-other BSs links) for joint detection. In Scenario II, these BSs are not synchronized and thus they can only utilize the target-reflected signals over their direct links for joint detection. For each of the two scenarios, we analyze the likelihood ratio test for detection and accordingly derive the detection probability subject to a required false alarm probability at any given target location, showing that the detection probability is monotonically increasing with respect to the total received reflection-signal power (over the utilized links for each scenario) at the BSs.
- Based on the derivation in each scenario and by considering each type of CU receivers, we propose the coordinated transmit beamforming design at the BSs to maximize the minimum detection probability (or equivalently the minimum total received reflection-signal power) over a particular targeted area, while satisfying the minimum SINR constraints at the CUs, subject to the maximum transmit power constraints at the BSs. These problems are recast as non-convex quadratically constrained quadratic programs (QCQPs), which are then optimally solved via the semi-definite relaxation (SDR) technique. In particular, we rigorously prove that the adopted SDRs are tight for these QCQPs and the optimal rank-one solutions for information beamforming can be properly constructed based on the optimal solution of the SDRs.
- Finally, we provide numerical results to validate the

performance of our proposed designs as compared to two benchmark schemes that perform ZF information beamforming and conduct the target detection only via dedicated sensing signals, respectively. It is shown that for each scenario, the proposed ISAC design achieves a higher detection probability than the benchmark schemes. It is also shown that ensuring time synchronization among BSs in Scenario I is consistently enhances the detection performance. Moreover, under both Scenario I and Scenario II, we show that Type-II CUs equipped with sensing interference cancellation capability outperform their Type-I counterparts and other benchmark designs in terms of detection performance, due to the higher flexibility in interference management of the Type-II CUs, which is always beneficial.

The remainder of this paper is organized as follows. Section II presents the networked ISAC system model. Section III derives the detection probability under a specific false alarm probability at any target location. Section IV presents the optimal coordinated transmit beamforming optimization problems for the two considered scenarios, respectively. Section V provides numerical results to validate the performance of our proposed schemes. Section VI concludes this paper.

Notations: Vectors and matrices are denoted by boldface lowercase and uppercase letters, respectively. $\mathbf{I}$ denotes an identity matrix with appropriate dimension. $\mathbb{E}(\cdot)$ denotes the statistical expectation. $\mathrm{var}\,(\cdot)$ denotes the statistical variance. For a scalar a, $|a|$ denotes its absolute value. For a vector $\mathbf{v}$, $\|\mathbf{v}\|$ denotes its Euclidean norm. For a matrix $\mathbf{M}$ of arbitrary dimension, $\mathbf{M}^T$ and $\mathbf{M}^H$ denote its transpose and conjugate transpose, respectively. $\mathbb{C}^{x \times y}$ denotes the space of $x \times y$ complex matrices. $\mathrm{Re}\,(\cdot)$ denotes the real part of a complex number, vector, or matrix. $\mathcal{N}(\mathbf{x}, \mathbf{Y})$ and $\mathcal{CN}(\mathbf{x}, \mathbf{Y})$ denote the real-valued Gaussian and the circularly symmetric complex Gaussian (CSCG) distributions with mean vector $\mathbf{x}$ and covariance matrix $\mathbf{Y}$, respectively, and "$\sim$" means "distributed as". $Q(\cdot)$ denotes the Q-function. $\mathrm{rank}\,(\cdot)$ denotes the rank of a matrix.
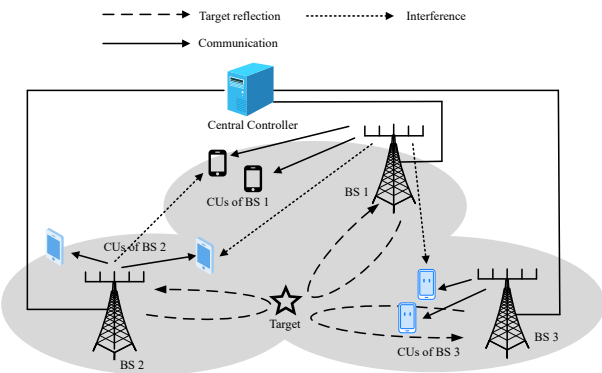

Fig. 1. An example of the considered multi-antenna networked ISAC system model with three coordinated BSs.

II. System Model

We consider a multi-antenna networked ISAC system consisting of L BSs each with $N_t > 1$ transmit and $N_r > 1$ receive antennas, where each BS serves the same number of K single-antenna CUs. Note that the total number of CUs is LK, let $\mathcal{L} \triangleq \{1, \ldots, L\}$ and $\mathcal{K}_l \triangleq \{1, \ldots, K\}$ denote the set of BSs and the set of CUs in each cell associated with BS l, respectively. In this system, the BSs send individual messages and dedicated sensing signals to their associated CUs. At the same time, the BSs receive and properly process the reflected signals and then convey them to a central controller (CC) for joint target detection, cf. Fig. 1. As such, the multi-antenna networked ISAC system unifies the multi-antenna coordinated beamforming system for communication [23] and the distributed MIMO radar for target detection [29], as will be detailed next. Specifically, we focus on the ISAC transmission over a communication block with duration T that consists of N symbols, where $T = NT_s$ with T_s denoting the duration of each symbol. Here, T or N is assumed to be sufficiently large for the ease of analysis [31]. Let $\mathcal{T} \triangleq (0, T]$ denote the ISAC period of interest and $\mathcal{N} \triangleq \{1, \ldots, N\}$ the set of symbols.

First, we consider the communication from the BSs to the CUs, in which the coordinated transmit beamforming is employed at these BSs. Let $\bar{s}_{l,i}(t) \in \mathbb{C}$ denote the communication signal sent by BS $l \in \mathcal{L}$ for CU $i \in \mathcal{K}_l$ at time $t \in \mathcal{T}$, $\mathbf{w}_{l,i} \in \mathbb{C}^{N_t \times 1}$ denote the corresponding transmit beamforming vector by BS $l \in \mathcal{L}$, and $\bar{\mathbf{s}}_l^r(t) \mathbb{C}^{N_t \times 1}$ denote the dedicated sensing signal sent by BS l at time t with zero mean and covariance matrix $\mathbf{R}_l^r = \mathbb{E}[\bar{\mathbf{s}}_l^r(t) \bar{\mathbf{s}}_l^{rH}(t)] \succeq \mathbf{0}$. With loss of generality, we assume $r_t = \mathrm{rank}(\mathbf{R}_l^r)$, As such, we express $\bar{\mathbf{s}}_l^r(t)$ as

$$\bar{\mathbf{s}}_l^r(t) = \sum_{k=1}^{r_t} \mathbf{w}_{l,k}^r \bar{s}_{l,k}^r(t), \tag{1}$$

where $\bar{s}_{l,k}^r(t)$ denotes the kth waveform of BS l that is modeled by an independently generated pseudorandom signal with zero mean and unit variance, and $\mathbf{w}_{l,k}^r$ denotes the corresponding transmit beamforming vector that can be determined based on $\mathbf{R}_l^r$ via eigenvalue decomposition (EVD). Denote $s_{l,i}[n]$, $s_{l,k}^r[n]$, and $\mathbf{s}_l^r[n]$ as the sampled signals of $\bar{s}_{l,i}(t)$, $\bar{s}_{l,k}^r(t)$, and $\bar{\mathbf{s}}_l^r(t)$, respectively, at each symbol $n \in \mathcal{N}$. Here, $\{s_{l,i}[n]\}$ are assumed to be independent and identically distributed (i.i.d.) random variables with zero mean and unit variance.

Let $\mathbf{h}_{l,m,i} \in \mathbb{C}^{N_t \times 1}$ denote the channel vector from BS $l \in \mathcal{L}$ to CU $i \in \mathcal{K}_m$ that is located in cell $m \in \mathcal{L}$. Then, the received signal by CU $k \in \mathcal{K}_m$ at cell m in symbol $n \in \mathcal{N}$ is

$$y_{m,k}[n] = \mathbf{h}_{m,m,k}^H \mathbf{w}_{m,k} s_{m,k}[n] + \underbrace{\sum_{i \in \mathcal{K}_m, i \neq k} \mathbf{h}_{m,m,k}^H \mathbf{w}_{m,i} s_{m,i}[n]}_{\mathrm{intra-cell\ interference}}$$

$$+ \underbrace{\sum_{l \in \mathcal{L}, l \neq m} \mathbf{h}_{l,m,k}^H \sum_{i \in \mathcal{K}_l} \mathbf{w}_{l,i} s_{l,i}[n]}_{\mathrm{inter-cell\ interference}} + \underbrace{\sum_{l \in \mathcal{L}} \mathbf{h}_{l,m,k}^H \mathbf{s}_l^r[n]}_{\mathrm{sensing\ interference}}$$

$$+ z_{m,k}[n], \tag{2}$$

where $z_{m,k}[n] \sim \mathcal{CN}\left(0, \sigma_c^2\right)$ denotes the noise at the receiver of CU k at cell m, with σ_c^2 denoting the corresponding noise power. It is observed in (2) that each CU suffers from both the intra-cell and inter-cell interference, as well as the interference from the dedicated sensing signals. In practice,

$$\gamma_{m,k}^{\mathrm{I}}\left(\{\mathbf{w}_{l,i}\},\{\mathbf{R}_l^r\}\right) = \frac{\left|\mathbf{h}_{m,m,k}^H \mathbf{w}_{m,k}\right|^2}{\displaystyle\sum_{i\in\mathcal{K}_m,i\neq k}\left|\mathbf{h}_{m,m,k}^H\mathbf{w}_{m,i}\right|^2 + \sum_{l\in\mathcal{L},l\neq m}\sum_{i\in\mathcal{K}_l}\left|\mathbf{h}_{l,m,k}^H\mathbf{w}_{l,i}\right|^2 + \sum_{l\in\mathcal{L}}\mathbf{h}_{l,m,k}^H\mathbf{R}_l^r\mathbf{h}_{l,m,k}+\sigma_c^2}. \tag{3}$$

$$\gamma_{m,k}^{\mathrm{II}}\left(\{\mathbf{w}_{l,i}\},\{\mathbf{R}_l^r\}\right) = \frac{\left|\mathbf{h}_{m,m,k}^H \mathbf{w}_{m,k}\right|^2}{\displaystyle\sum_{i\in\mathcal{K}_m,i\neq k}\left|\mathbf{h}_{m,m,k_m}^H\mathbf{w}_{m,i_m}\right|^2 + \sum_{l\in\mathcal{L},l\neq m}\sum_{i\in\mathcal{K}_l}\left|\mathbf{h}_{l,m,k}^H\mathbf{w}_{l,i}\right|^2 + \sigma_c^2}. \tag{4}$$

the noise term $z_{m,k}[n]$ may also include the background and clutter interference [41]. Notice that $\{\bar{\mathbf{s}}_l^r(t)\}$ are predetermined pseudorandom signals that can be *a-priori* known by all the BSs and CUs. Therefore, we consider two different types of CUs: those without the capability of canceling the interference caused by the dedicated sensing signal [16], referred to as Type-I receivers, and those with the capability, referred to as Type-II receivers, respectively.

Type-I receivers: Each Type-I receiver k in cell m is not equipped with the capability to cancel the interference generated by the dedicated sensing signal $\mathbf{s}_l^r[n]$. The SINR of CU k in cell m is given by (3).

Type-II receivers: Each Type-II receiver k in cell m is dedicatedly designed for the ISAC system with the capability to cancel the interference generated by dedicated sensing signal $\mathbf{s}_l^r[n]$ before decoding its desired communication signal $s_{m,k}[n]$. In this case, the SINR of CU k in cell m is given by (4).

Next, we consider the distributed MIMO radar detection by the L BSs via reusing both the communication signals $\{\bar{s}_{l,i}(t)\}$ and the dedicated sensing signals $\{\bar{\mathbf{s}}_l^r(t)\}$ concurrently. Let (x_l, y_l) denote the location of each BS $l \in \mathcal{L}$. Suppose that there is one target present at location (x_0, y_0), for which the target angle with respect to BS l is denoted by θ_l. Let $\mathbf{a}_{t,l}(\theta_l) \in \mathbb{C}^{N_t \times 1}$ and $\mathbf{a}_{r,l}(\theta_l) \in \mathbb{C}^{N_r \times 1}$ denote the transmit and receive steering vectors at BS $l \in \mathcal{L}$, respectively, where $\|\mathbf{a}_{t,l}(\theta_l)\|/N_t = \|\mathbf{a}_{r,l}(\theta_l)\|/N_r = 1$ is assumed without loss of generality [16]. In the practical case with uniform linear arrays (ULAs) deployed at the BSs, we have

$$\mathbf{a}_{t,l}(\theta_l) = \left[1, e^{j2\pi\frac{d_a}{\lambda}\sin(\theta_l)}, \ldots, e^{j2\pi\frac{d_a}{\lambda}(N_t-1)\sin(\theta_l)}\right]^T, \tag{5}$$

and

$$\mathbf{a}_{r,l}(\theta_l) = \left[1, e^{j2\pi\frac{d_a}{\lambda}\sin(\theta_l)}, \ldots, e^{j2\pi\frac{d_a}{\lambda}(N_r-1)\sin(\theta_l)}\right]^T, \tag{6}$$

where $j = \sqrt{-1}$, while parameters d_a and λ denote the antenna spacing and wavelength, respectively. Let $\mathbf{H}_{m,l} = \hat{\zeta}_{m,l}\mathbf{a}_{r,m}(\theta_m)\mathbf{a}_{t,l}^T(\theta_l) \in \mathbb{C}^{N_r \times N_t}$ denote the end-to-end target response matrix from BS l-to-the-target-to-BS m, in which $\hat{\zeta}_{m,l} = \sqrt{\beta_{m,l}}\zeta_{m,l}$ is the reflection coefficient incorporating both the RCS $\zeta_{m,l}$ and the equivalent round-trip path loss $\beta_{m,l}$. Specifically, we assume that $\beta_{m,l} = \kappa^2\frac{d_{\mathrm{ref}}^4}{d_m^2 d_l^2}$, where κ denotes the path loss at the reference distance d_{ref} and $d_l = \sqrt{(x_l-x_0)^2 + (y_l-y_0)^2}$ denotes the distance between

the target and BS m. As such, the received echo signal at BS m is

$$\mathbf{r}_m(t) = \sum_{l\in\mathcal{L}}\mathbf{H}_{m,l}\left(\sum_{i\in\mathcal{K}_l}\mathbf{w}_{l,i}\bar{s}_{l,i}(t-\tau_{m,l}) + \bar{\mathbf{s}}_l^r(t-\tau_{m,l})\right) + \bar{\mathbf{z}}_m(t), \tag{7}$$

where $\bar{\mathbf{z}}_m(t) \sim \mathcal{CN}\left(\mathbf{0}, \sigma_d^2\mathbf{I}\right)$ denotes the noise at the receiver of BS m and $\tau_{m,l} = \frac{1}{c}(d_m + d_l)$ denotes the transmission delay from BS l-to-the-target-to-BS m, with c denoting the speed of light. Without loss of generality, we assume that each information signal and dedicated sensing signal have a normalized power over block $\mathcal{T}$, i.e., $\frac{1}{T}\int_{\mathcal{T}}|\bar{s}_{l,i}(t)|^2 dt = 1$ and $\frac{1}{T}\int_{\mathcal{T}}\left|\bar{s}_{l,k}^r(t)\right|^2 dt = 1$. Furthermore, notice that $\{\bar{s}_{l,i}(t)\}$ and $\{\bar{s}_{l,k}^r(t)\}$ are with zero mean and independent over different CUs and different times. As T is sufficiently large, we have $\frac{1}{T}\int_{\mathcal{T}}\bar{s}_{l,i}(t)\bar{s}_{m,k}^*(t-\tau)dt = 0, \forall\tau, l \neq m, k \neq i$, and $\frac{1}{T}\int_{\mathcal{T}}\bar{s}_{l,k}^r(t)\bar{s}_{m,i}^{r*}(t-\tau)dt = 0, \forall\tau, l \neq m, k \neq i$, as well as $\frac{1}{T}\int_{\mathcal{T}}\bar{s}_{l,i}(t)\bar{s}_{l,i}^*(t-\tau)dt = 0$ and $\frac{1}{T}\int_{\mathcal{T}}\bar{s}_{l,i}^r(t)\bar{s}_{l,i}^{r*}(t-\tau)dt = 0$ for any l, i and $|\tau| \geq T_s$. Based on the received signals $\{\mathbf{r}_m(t)\}$ in (7), the L BSs jointly detect the existence of the target, as will be illustrated in the next section.

III. DETECTION PROBABILITY AT GIVEN TARGET LOCATION

In this section, we derive the detection probability and the false alarm probability at a given target location (x_0, y_0), by particularly considering the two joint detection scenarios with and without time synchronization among the BSs, namely Scenario-I and Scenario-II, respectively.

Scenario I: All the BSs are synchronized in time such that the mutual delays $\tau_{m,l}$ are known. As such, the target-reflected signals over both the direct links (i.e., $\mathbf{H}_{m,m}(\sum_{i\in\mathcal{K}_m}\mathbf{w}_{m,i}\bar{s}_{m,i}(t-\tau_{m,m}) + \bar{\mathbf{s}}_m^r(t-\tau_{m,m}))$ from each BS m-to-the-target-to-originated BS) and the cross links (i.e., $\mathbf{H}_{m,l}(\sum_{i\in\mathcal{K}_l}\mathbf{w}_{l,i}\bar{s}_{l,i}(t-\tau_{m,l}) + \bar{\mathbf{s}}_l^r(t-\tau_{m,l}))$ from other BSs l's-to-the-target-to-BS m, $\forall l \neq m$) can be exploited for joint detection. Towards this end, each BS m performs the matched filtering (MF) processing based on $\mathbf{r}_m(t)$ by exploit-

$$\mathbf{d}_{\mathrm{I}} = \left[\mathbf{d}_{1,1,1}^T, \ldots, \mathbf{d}_{1,1,K}^T, \mathbf{d}_{1,2,1}^T, \ldots, \mathbf{d}_{L,L,K}^T, \mathbf{d}_{1,1,1}^{rT}, \ldots, \mathbf{d}_{1,1,r_t}^{rT}, \mathbf{d}_{1,2,1}^{rT}, \ldots, \mathbf{d}_{L,L,r_t}^{rT}\right]^T \in \mathbb{C}^{N_r(K+r_t)L^2}. \tag{10}$$

$$\mathbf{d}_{\mathrm{II}} = \left[\mathbf{d}_{1,1,1}^T, \ldots, \mathbf{d}_{1,1,K}^T, \mathbf{d}_{2,2,1}^T, \ldots, \mathbf{d}_{L,L,K}^T, \mathbf{d}_{1,1,1}^{rT}, \ldots, \mathbf{d}_{1,1,r_t}^{rT}, \mathbf{d}_{2,2,1}^{rT}, \ldots, \mathbf{d}_{L,L,r_t}^{rT}\right]^T \in \mathbb{C}^{N_r(K+r_t)L}. \tag{11}$$

ing $\{\bar{s}_{l,i}(t)\}$, $\{\bar{s}_{l,k}^r(t)\}$, and delay $\{\tau_{m,l}\}$. Accordingly, the processed signal based on $\bar{s}_{l,i}(t)$ is

$$\begin{aligned}
\mathbf{d}_{m,l,i} &= \frac{1}{T} \int_{\mathcal{T}} \mathbf{r}_m(t)\, \bar{s}_{l,i}^*(t - \tau_{m,l})\, dt \\
&= \underbrace{\frac{1}{T} \int_{\mathcal{T}} \mathbf{H}_{m,l} \mathbf{w}_{l,i} \left|\bar{s}_{l,i}^*(t - \tau_{m,l})\right|^2 dt}_{\text{desired signal}} \\
&\quad + \underbrace{\frac{1}{T} \int_{\mathcal{T}} \mathbf{z}_m(t)\, \bar{s}_{l,i}^*(t - \tau_{m,l})\, dt}_{\text{filtered noise}} \\
&= \mathbf{H}_{m,l} \mathbf{w}_{l,i} + \hat{\mathbf{z}}_{m,l,i}.
\end{aligned} \tag{8}$$

Similarly, the processed signal based on $\bar{s}_{l,k}^r(t)$ is

$$\begin{aligned}
\mathbf{d}_{m,l,k}^r &= \frac{1}{T} \int_{\mathcal{T}} \mathbf{r}_m(t)\, \bar{s}_{l,k}^{r*}(t - \tau_{m,l})\, dt \\
&= \underbrace{\frac{1}{T} \int_{\mathcal{T}} \mathbf{H}_{m,l} \mathbf{w}_{l,k}^r \left|\bar{s}_{l,k}^{r*}(t - \tau_{m,l})\right|^2 dt}_{\text{desired signal}} \\
&\quad + \underbrace{\frac{1}{T} \int_{\mathcal{T}} \mathbf{z}_m(t)\, \bar{s}_{l,k}^{r*}(t - \tau_{m,l})\, dt}_{\text{filtered noise}} \\
&= \mathbf{H}_{m,l} \mathbf{w}_{l,k}^r + \hat{\mathbf{z}}_{m,l,k}^r.
\end{aligned} \tag{9}$$

In (8) and (9), $\hat{\mathbf{z}}_{m,l,i} \sim \mathcal{CN}\left(\mathbf{0}, \sigma_d^2 \mathbf{I}\right)$ and $\hat{\mathbf{z}}_{m,l,k}^r \sim \mathcal{CN}\left(\mathbf{0}, \sigma_d^2 \mathbf{I}\right)$ denote the equivalent noise after MF processing, where σ_d^2 is the per-antenna noise power at each BS. After obtaining $\{\mathbf{d}_{m,l,i}\}_{l \in \mathcal{L}}$ and $\{\mathbf{d}_{m,l,k}^r\}_{l \in \mathcal{L}}$, each BS m delivers them to the CC, which then performs the joint radar detection based on $\{\mathbf{d}_{m,l,i}\}$ and $\{\mathbf{d}_{m,l,k}^r\}$. For ease of illustration, the observed signals can be stacked as (10).

Scenario II: In this scenario, the BSs are not synchronized in time and thus the value of transmission delay $\tau_{m,l}$ with respect to other BS $l \neq m$ is not available at BS m. In this scenario, the BSs can only utilize the target-reflected signals over their direct links, i.e., $(\mathbf{H}_{m,m}(\sum_{i \in \mathcal{K}_m} \mathbf{w}_{m,i} \bar{s}_{m,i}(t - \tau_{m,m}) + \mathbf{s}_m^r(t - \tau_{m,m})), \forall m \in \mathcal{L})$, for joint detection. After the MF processing similarly as in Scenario I, we have the processed signal as (11), where $\{\mathbf{d}_{m,l,i}\}$ and $\{\mathbf{d}_{m,l,k}^r\}$ are defined as (8) and (9), respectively.

A. Detection Probability in Scenario I with BSs Synchronization

To start with, we define two hypotheses for target detection, i.e., $\mathcal{H}_1$ when the target exists and $\mathcal{H}_0$ when the target does not exist. For notational simplicity, we define $\boldsymbol{\alpha}_{m,l,i}^c = \mathbf{H}_{m,l} \mathbf{w}_{l,i}$ and $\boldsymbol{\alpha}_{m,l,k}^r = \mathbf{H}_{m,l} \mathbf{w}_{l,k}^r$ as the reflected communication signal and dedicated sensing signal vectors from BS l-to-the target-to-BS m when the target exists. Also, we present the correspondingly accumulated signal vector as (12). Furthermore, define the noise vector in Scenario I as (13). Then, based on (8), we have the processed signals after the MF processing as

$$\left\{ \begin{array}{l} \mathcal{H}_1 : \mathbf{d}_{\mathrm{I}} = \boldsymbol{\alpha}_{\mathrm{I}} + \hat{\mathbf{z}}_{\mathrm{I}}, \\ \mathcal{H}_0 : \mathbf{d}_{\mathrm{I}} = \hat{\mathbf{z}}_{\mathrm{I}}. \end{array} \right. \tag{14}$$

Next, we adopt the likelihood ratio test for target detection. Based on (14), the likelihood functions of vector $\mathbf{d}_{\mathrm{I}}$ under the hypothesis $\mathcal{H}_1$ and $\mathcal{H}_0$ are respectively given by

$$p\left(\mathbf{d}_{\mathrm{I}} | \mathcal{H}_1\right) = c_0 \exp\left(-\frac{1}{\sigma_d^2} (\mathbf{d}_{\mathrm{I}} - \boldsymbol{\alpha}_{\mathrm{I}})^H (\mathbf{d}_{\mathrm{I}} - \boldsymbol{\alpha}_{\mathrm{I}})\right), \tag{15}$$

$$p\left(\mathbf{d}_{\mathrm{I}} | \mathcal{H}_0\right) = c_0 \exp\left(-\frac{1}{\sigma_d^2} \mathbf{d}_{\mathrm{I}}^H \mathbf{d}_{\mathrm{I}}\right), \tag{16}$$

where $c_0 = \frac{1}{\pi^{N_r(K+r_t)L^2} \sigma_d^{2N_r(K+r_t)L^2}}$. Accordingly, the Neyman-Pearson (NP) detector is given by the likelihood ratio test [42]:

$$\ln \frac{p\left(\mathbf{d}_{\mathrm{I}} | \mathcal{H}_1\right)}{p\left(\mathbf{d}_{\mathrm{I}} | \mathcal{H}_0\right)} = \frac{1}{\sigma_d^2} \left(2\mathrm{Re}\left(\boldsymbol{\alpha}_{\mathrm{I}}^H \mathbf{d}_{\mathrm{I}}\right) - \boldsymbol{\alpha}_{\mathrm{I}}^H \boldsymbol{\alpha}_{\mathrm{I}}\right) \underset{\mathcal{H}_0}{\overset{\mathcal{H}_1}{\gtrless}} \delta, \tag{17}$$

where δ denotes the threshold determined by the tolerable level of false alarm. Notice that since $\boldsymbol{\alpha}_{\mathrm{I}}^H \boldsymbol{\alpha}_{\mathrm{I}}$ is given, the detector in (17) can be equivalently simplified as

$$T\left(\mathbf{d}_{\mathrm{I}}\right) = \mathrm{Re}\left(\boldsymbol{\alpha}_{\mathrm{I}}^H \mathbf{d}_{\mathrm{I}}\right) \underset{\mathcal{H}_0}{\overset{\mathcal{H}_1}{\gtrless}} \delta', \tag{18}$$

where δ' denotes the threshold related to $T\left(\mathbf{d}_{\mathrm{I}}\right)$.

Then, we derive the distribution of $T\left(\mathbf{d}_{\mathrm{I}}\right)$. Towards this end, we consider $x = \boldsymbol{\alpha}_{\mathrm{I}}^H \mathbf{d}_{\mathrm{I}}$, whose expectation and variance under hypothesis $\mathcal{H}_1$ and $\mathcal{H}_0$ are respectively obtained as

$$\mathbb{E}\left(x | \mathcal{H}_0\right) = 0, \tag{19}$$

$$\begin{aligned}
\mathbb{E}\left(x | \mathcal{H}_1\right) &= \mathcal{E}_{\mathrm{I}} \triangleq \sum_{l \in \mathcal{L}} \sum_{m \in \mathcal{L}} \left(\sum_{i \in \mathcal{K}_l} \|\mathbf{H}_{m,l} \mathbf{w}_{l,i}\|^2 \right. \\
&\quad \left. + \sum_{k=1}^{r_t} \|\mathbf{H}_{m,l} \mathbf{w}_{l,k}^r\|^2\right) \\
&= N_r \sum_{l \in \mathcal{L}} \sum_{m \in \mathcal{L}} \zeta_{m,l}^2 \beta_{m,l} (\sum_{i \in \mathcal{K}_l} \left|\mathbf{a}_{t,l}^T(\theta_l) \mathbf{w}_{l,i}\right|^2 \\
&\quad + \mathbf{a}_{t,l}^T(\theta_l) \mathbf{R}_l^r \mathbf{a}_{t,l}(\theta_l)),
\end{aligned} \tag{20}$$

$$\mathrm{var}\left(x | \mathcal{H}_0\right) = \mathrm{var}\left(x | \mathcal{H}_1\right) = \sigma_d^2 \mathcal{E}_{\mathrm{I}}. \tag{21}$$

By combining (19), (20), and (21), we have

$$\left\{ \begin{array}{l} x \sim \mathcal{CN}\left(0, \sigma_d^2 \mathcal{E}_{\mathrm{I}}\right), \mathcal{H}_0, \\ x \sim \mathcal{CN}\left(\mathcal{E}_{\mathrm{I}}, \sigma_d^2 \mathcal{E}_{\mathrm{I}}\right), \mathcal{H}_1. \end{array} \right. \tag{22}$$

$$\boldsymbol{\alpha}_{\mathrm{I}} = \left[\boldsymbol{\alpha}_{1,1,1}^{cT}, \ldots, \boldsymbol{\alpha}_{1,1,K}^{cT}, \boldsymbol{\alpha}_{1,2,1}^{cT}, \ldots, \boldsymbol{\alpha}_{L,L,K}^{cT}, \boldsymbol{\alpha}_{1,1,1}^{rT}, \ldots, \boldsymbol{\alpha}_{1,1,r_t}^{rT}, \boldsymbol{\alpha}_{1,2,1}^{rT}, \ldots, \boldsymbol{\alpha}_{L,L,r_t}^{rT} \right]^T \in \mathbb{C}^{N_r(K+r_t)L^2}. \tag{12}$$

$$\hat{\mathbf{z}}_{\mathrm{I}} = \left[\hat{\mathbf{z}}_{1,1,1}^{T}, \ldots, \hat{\mathbf{z}}_{1,1,K}^{T}, \hat{\mathbf{z}}_{1,2,1}^{T}, \ldots, \hat{\mathbf{z}}_{L,L,K}^{T}, \hat{\mathbf{z}}_{1,1,1}^{rT}, \ldots, \hat{\mathbf{z}}_{1,1,r_t}^{rT}, \hat{\mathbf{z}}_{1,2,1}^{rT}, \ldots, \hat{\mathbf{z}}_{L,L,r_t}^{rT} \right]^T \in \mathbb{C}^{N_r(K+r_t)L^2}. \tag{13}$$

As a result, for $T(\mathbf{d}_{\mathrm{I}}) = \mathrm{Re}(x)$, it follows that

$$\begin{cases} T(\mathbf{d}_{\mathrm{I}}) \sim \mathcal{N}\left(0, \sigma_d^2 \mathcal{E}_{\mathrm{I}}/2\right), \mathcal{H}_0, \\ T(\mathbf{d}_{\mathrm{I}}) \sim \mathcal{N}\left(\mathcal{E}_{\mathrm{I}}, \sigma_d^2 \mathcal{E}_{\mathrm{I}}/2\right), \mathcal{H}_1. \end{cases} \tag{23}$$

Finally, we derive the detection probability under a required false alarm probability. Based on (18) and (23), we obtain the detection probability $p_{\mathrm{D}}^{\mathrm{I}}$ and the false alarm probability $p_{\mathrm{FA}}^{\mathrm{I}}$ with respect to the detector threshold δ' as

$$p_{\mathrm{D}}^{\mathrm{I}} = Q\left((\delta' - \mathcal{E}_{\mathrm{I}})\sqrt{\frac{2}{\sigma_d^2 \mathcal{E}_{\mathrm{I}}}}\right), \tag{24}$$

$$p_{\mathrm{FA}}^{\mathrm{I}} = Q\left(\delta'\sqrt{\frac{2}{\sigma_d^2 \mathcal{E}_{\mathrm{I}}}}\right), \tag{25}$$

respectively. Based on (25), we have $\delta'\sqrt{\frac{2}{\sigma_d^2 \mathcal{E}_{\mathrm{I}}}} = Q^{-1}\left(p_{\mathrm{FA}}^{\mathrm{I}}\right)$. By substituting this into (24), we obtain the detection probability for given false alarm probability $p_{\mathrm{FA}}^{\mathrm{I}}$ as

$$p_{\mathrm{D}}^{\mathrm{I}} = Q\left(Q^{-1}\left(p_{\mathrm{FA}}^{\mathrm{I}}\right) - \sqrt{\frac{2\mathcal{E}_{\mathrm{I}}}{\sigma_d^2}}\right). \tag{26}$$

It is observed that the detection probability $p_{\mathrm{D}}^{\mathrm{I}}$ in (26) is monotonically increasing with respect to $\mathcal{E}_{\mathrm{I}}$ in (20), which corresponds to the total received reflection-signal power over both direct and cross reflection links. Denote $\mathbf{A}_l(\theta_l) = \mathbf{a}_{t,l}^*(\theta_l)\mathbf{a}_{t,l}^T(\theta_l), \forall l \in \mathcal{L}$, $\mathcal{E}_{\mathrm{I}}$ is reexpressed as

$$\mathcal{E}_{\mathrm{I}} = N_r \sum_{l \in \mathcal{L}} \sum_{m \in \mathcal{L}} \zeta_{m,l}^2 \beta_{m,l} \left(\sum_{i \in \mathcal{K}_l} \mathrm{tr}\left(\mathbf{w}_{l,i}\mathbf{w}_{l,i}^H \mathbf{A}_l(\theta_l)\right) + \mathrm{tr}\left(\mathbf{R}_l^r \mathbf{A}_l(\theta_l)\right) \right). \tag{27}$$

As a result, maximizing the detection performance of the system is equivalent to maximizing the received reflection-signal power $\mathcal{E}_{\mathrm{I}}$ in (27).

B. Detection Probability in Scenario II without BSs Synchronization

Next, we consider Scenario II without synchronization among the BSs. The detection probability in this scenario can be similarly derived as that in Scenario I, by replacing $\mathbf{d}_{\mathrm{I}}$ by $\mathbf{d}_{\mathrm{II}}$ and accordingly replacing $\mathcal{E}_{\mathrm{I}}$ in (20) by

$$\begin{aligned} \mathcal{E}_{\mathrm{II}} &= N_r \sum_{m \in \mathcal{L}} \zeta_{m,m}^2 \beta_{m,m} \left(\sum_{i \in \mathcal{K}_m} \left| \mathbf{a}_{t,m}^T(\theta_m)\mathbf{w}_{m,i} \right|^2 \right. \\ &\quad \left. + \mathbf{a}_{t,m}^T(\theta_l)\mathbf{R}_m^r \mathbf{a}_{t,m}(\theta_m) \right) \\ &= N_r \sum_{m \in \mathcal{L}} \zeta_{m,m}^2 \beta_{m,m} \left(\sum_{i \in \mathcal{K}_m} \mathrm{tr}\left(\mathbf{w}_{m,i}\mathbf{w}_{m,i}^H \mathbf{A}_m(\theta_m)\right) \right. \\ &\quad \left. + \mathrm{tr}\left(\mathbf{R}_m^r \mathbf{A}_m(\theta_m)\right) \right), \end{aligned} \tag{28}$$

where $\mathbf{A}_m(\theta_m) = \mathbf{a}_{t,m}^*(\theta_m)\mathbf{a}_{t,m}^T(\theta_m), \forall m \in \mathcal{L}$.

Based on the similar derivation procedure as in Section III-A, we have the detection probability $p_{\mathrm{D}}^{\mathrm{II}}$ for a given false alarm probability $p_{\mathrm{FA}}^{\mathrm{II}}$ as

$$p_{\mathrm{D}}^{\mathrm{II}} = Q\left(Q^{-1}\left(p_{\mathrm{FA}}^{\mathrm{II}}\right) - \sqrt{\frac{2\mathcal{E}_{\mathrm{II}}}{\sigma_d^2}}\right). \tag{29}$$

It is observed from (29) that the detection probability $p_{\mathrm{D}}^{\mathrm{II}}$ is monotonically increasing with respect to the total received reflection-signal power over the direct links only, i.e., $\mathcal{E}_{\mathrm{II}}$ in (28). Therefore, maximizing $p_{\mathrm{D}}^{\mathrm{II}}$ is equivalent to maximizing the received reflection-signal power $\mathcal{E}_{\mathrm{II}}$ in (29).

IV. SINR-CONSTRAINED DETECTION PROBABILITY MAXIMIZATION VIA COORDINATED TRANSMIT BEAMFORMING

In this section, we design the coordinated transmit beamforming $\{\mathbf{w}_{l,k}\}$ and dedicated sensing signal covariance matrix $\{\mathbf{R}_l^r\}$ to maximize the minimum detection probability with a given false alarm probability p_{FA} over a particular targeted area, subject to the minimum SINR requirement $\Gamma_{m,k}$ at each cell $m \in \mathcal{L}$ and CU $k \in \mathcal{K}_m$, and the maximum power constraint $P_{\max}$ at each BS. In particular, let $\mathcal{Q}$ denote the targeted area for detection. To facilitate the design, we select Q sample locations from $\mathcal{Q}$, denoted by $(x_0^{(q)}, y_0^{(q)}), \forall q \in \mathcal{Q} \triangleq \{1, \ldots, Q\}$. For a potential target located at $(x_0^{(q)}, y_0^{(q)})$, we denote the target angle with respect to BS $l \in \mathcal{L}$ as $\theta_l^{(q)}$ and the round-trip path loss from BS $l \in \mathcal{L}$ to target to BS $m \in \mathcal{L}$ as $\beta_{m,l}^{(q)}$.

A. Scenario I with BSs Synchronization

First, we consider Scenario I with BSs synchronization. In this scenario, for given target location q, maximizing the detection probability in this scenario is equivalent to maximizing $\mathcal{E}_{\mathrm{I}}$ in (27). Based on this observation, the SINR-constrained minimum detection probability maximization problems over the given targeted area with Type-I and Type-II receivers are formulated as

$$(\mathrm{P1}): \max_{\{\mathbf{w}_{l,i}, \mathbf{R}_l^r\}} \min_{q \in \mathcal{Q}} f^{\mathrm{I}}\left(\{\mathbf{w}_{l,i}\}, \{\mathbf{R}_l^r\}\right) \tag{30a}$$

$$\mathrm{s.t.} \quad \gamma_{m,k}^{\mathrm{I}}\left(\{\mathbf{w}_{l,i}\}, \{\mathbf{R}_l^r\}\right) \geq \Gamma_{m,k},$$
$$\forall k \in \mathcal{K}_m, \forall m \in \mathcal{L}, \tag{30b}$$

$$\sum_{i \in \mathcal{K}_l} \|\mathbf{w}_{l,i}\|^2 + \mathrm{Tr}(\mathbf{R}_l^r) \leq P_{\max}, \forall l \in \mathcal{L}, \tag{30c}$$

$$\mathbf{R}_l^r \succeq \mathbf{0}, \forall l \in \mathcal{L}, \tag{30d}$$

and

$$(\text{P2}): \max_{\{\mathbf{w}_{l,i}, \mathbf{R}_l^r\}} \min_{q \in \mathcal{Q}} f^{\text{I}}\left(\{\mathbf{w}_{l,i}\}, \{\mathbf{R}_l^r\}\right) \tag{31a}$$

$$\text{s.t.} \quad \gamma_{m,k}^{\text{II}}\left(\{\mathbf{w}_{l,i}\}, \{\mathbf{R}_l^r\}\right) \geq \Gamma_{m,k},$$
$$\forall k \in \mathcal{K}_m, \forall m \in \mathcal{L}, \tag{31b}$$
$$(30c) \text{ and } (30d),$$

respectively, where

$$f^{\text{I}}\left(\{\mathbf{w}_{l,i}\}, \{\mathbf{R}_l^r\}\right) = \sum_{l \in \mathcal{L}} \sum_{m \in \mathcal{L}} \zeta_{m,l}^2 \beta_{m,l}^{(q)} \text{tr}((\sum_{i \in \mathcal{K}_l} \mathbf{w}_{l,i}\mathbf{w}_{l,i}^H$$
$$+ \mathbf{R}_l^r)\mathbf{A}_l(\theta_l^{(q)})), \tag{32}$$

(30b) and (31b) denote the minimum SINR constraints at different types of CUs and (30c) denotes the maximum transmit power constraints at the BSs. Notice that problems (P1) and (P2) are non-convex due to the non-convex constraints in (30b) and (31b). In the following, we apply the SDR technique to solve problems (P1) and (P2).

Towards this end, we introduce Ω as an auxiliary optimization variable and define $\mathbf{W}_{l,i} = \mathbf{w}_{l,i}\mathbf{w}_{l,i}^H \succeq \mathbf{0}$ with $\text{rank}(\mathbf{W}_{l,i}) \leq 1, \forall l \in \mathcal{L}, i \in \mathcal{K}_l$. Problems (P1) and (P2) are equivalently reformulated as

$$(\text{P1.1}): \max_{\{\mathbf{W}_{l,i} \succeq \mathbf{0}, \mathbf{R}_l^r \succeq \mathbf{0}, \Omega\}} \Omega \tag{33a}$$

$$\text{s.t.} \quad \hat{f}^{\text{I}}\left(\{\mathbf{W}_{l,i}\}, \{\mathbf{R}_l^r\}\right) \geq \Omega, \forall q \in \mathcal{Q}, \tag{33b}$$

$$\sum_{l \in \mathcal{L}} \sum_{i \in \mathcal{K}_l} \text{tr}\left(\mathbf{h}_{l,m,k}\mathbf{h}_{l,m,k}^H \mathbf{W}_{l,i}\right)$$
$$+ \sum_{l \in \mathcal{L}} \text{tr}\left(\mathbf{h}_{l,m,k}\mathbf{h}_{l,m,k}^H \mathbf{R}_l^r\right)$$
$$+ \sigma_c^2 \leq (1 + \frac{1}{\Gamma_{m,k}})\text{tr}\left(\mathbf{h}_{m,m,k}\mathbf{h}_{m,m,k}^H \mathbf{W}_{m,k}\right),$$
$$\forall k \in \mathcal{K}_m, \forall m \in \mathcal{L}, \tag{33c}$$

$$\sum_{i \in \mathcal{K}_l} \text{tr}\left(\mathbf{W}_{l,i}\right) + \text{tr}(\mathbf{R}_l^r) \leq P_{\max}, \forall l \in \mathcal{L}, \tag{33d}$$

$$\text{rank}(\mathbf{W}_{l,i}) \leq 1, \forall i \in \mathcal{K}_l, \forall l \in \mathcal{L} \tag{33e}$$

and

$$(\text{P2.1}): \max_{\{\mathbf{W}_{l,i} \succeq \mathbf{0}, \mathbf{R}_l^r \succeq \mathbf{0}, \Omega\}} \Omega \tag{34a}$$

$$\text{s.t.} \quad \sum_{l \in \mathcal{L}} \sum_{i \in \mathcal{K}_l} \text{tr}\left(\mathbf{h}_{l,m,k}\mathbf{h}_{l,m,k}^H \mathbf{W}_{l,i}\right) + \sigma_c^2$$

$$\leq \left(1 + \frac{1}{\Gamma_{m,k}}\right) \text{tr}\left(\mathbf{h}_{m,m,k}\mathbf{h}_{m,m,k}^H \mathbf{W}_{m,k}\right),$$
$$\forall k \in \mathcal{K}_m, \forall m \in \mathcal{L}, \tag{34b}$$
$$(33b), (33d), \text{ and } (33e),$$

respectively, where

$$\hat{f}^{\text{I}}\left(\{\mathbf{W}_{l,i}\}, \{\mathbf{R}_l^r\}\right) = \sum_{l \in \mathcal{L}} \sum_{m \in \mathcal{L}} \zeta_{m,l}^2 \beta_{m,l}^{(q)} \text{tr}((\sum_{i \in \mathcal{K}_l} \mathbf{W}_{l,i}$$
$$+ \mathbf{R}_l^r)\mathbf{A}_l(\theta_l^{(q)})) \tag{35}$$

However, problems (P1.1) and (P2.1) are still non-convex due to the rank-one constraints in (33e). To tackle this issue,

we drop these rank-one constraints and obtain the SDR version of (P1.1) and (P2.1) as (SDR1.1) and (SDR2.1) [43] respectively, both of them are convex and can be optimally solved by standard convex optimization program solvers such as CVX [44]. Let $\{\{\mathbf{W}_{l,i}^*\}, \{\mathbf{R}_l^{r*}\}, \Omega^*\}$ and $\{\{\mathbf{W}_{l,i}^{**}\}, \{\mathbf{R}_l^{r**}\}, \Omega^{**}\}$ denote the optimal solutions to (SDR1.1) and (SDR2.1), respectively. Notice that the obtained $\mathbf{W}_{l,i}^*$ and $\mathbf{W}_{l,i}^{**}$ are generally of high ranks, which do not necessarily satisfy the rank-one constraints in (P1.1) and (P2.1). As such, we introduce the following additional step to construct the equivalent optimal rank-one solutions to (P1.1) and (P2.1).

Proposition 1: The SDR of problem (P1.1) is tight. In particular, based on the optimal solution of $\{\{\mathbf{W}_{l,i}^*\}, \{\mathbf{R}_l^{r*}\}, \Omega^*\}$ to (SDR1.1), if any of $\{\mathbf{W}_{l,i}^*\}$ is not rank-one, we can always construct the equivalent optimal rank-one solution of $\{\{\tilde{\mathbf{W}}_{l,i}\}, \{\tilde{\mathbf{R}}_l^r\}, \tilde{\Omega}\}$ to (P1.1) according to the following, which achieves the same objective value as (SDR1.1):

$$\tilde{\mathbf{w}}_{l,i} = \left(\mathbf{h}_{l,m,k}^H \mathbf{W}_{l,i}^* \mathbf{h}_{l,m,k}\right)^{-\frac{1}{2}} \mathbf{W}_{l,i}^* \mathbf{h}_{l,m,k}, \tag{36a}$$

$$\tilde{\mathbf{W}}_{l,i} = \tilde{\mathbf{w}}_{l,i}\tilde{\mathbf{w}}_{l,i}^H, \tag{36b}$$

$$\tilde{\mathbf{R}}_l^r = \sum_{i \in \mathcal{K}_l} \mathbf{W}_{l,i}^* + \tilde{\mathbf{R}}_l^{r*} - \sum_{i \in \mathcal{K}_l} \tilde{\mathbf{W}}_{l,i}^* \tag{36c}$$

$$\tilde{\Omega} = \Omega^*. \tag{36d}$$

proof 1: See Appendix A.

Similarly as for problem (P1.1), we find the optimal solution to (P2.1) by showing that the SDR is tight in the following proposition.

Proposition 2: The SDR of problem (P2.1) is tight. In particular, based on the optimal solution of $\{\{\mathbf{W}_{l,i}^{**}\}, \{\mathbf{R}_l^{r**}\}, \Omega^{**}\}$ to (SDR2.1), if any of $\{\mathbf{W}_{l,i}^{**}\}$ is not rank-one, we can always construct the equivalent optimal rank-one solution of $\{\{\bar{\mathbf{W}}_{l,i}\}, \{\bar{\mathbf{R}}_l^r\}, \bar{\Omega}\}$ to (P2.1) in the following, which achieves the same objective value as (SDR2.1):

$$\bar{\mathbf{w}}_{l,i} = \left(\mathbf{h}_{l,m,k}^H \mathbf{W}_{l,i}^{**} \mathbf{h}_{l,m,k}\right)^{-\frac{1}{2}} \mathbf{W}_{l,i}^{**} \mathbf{h}_{l,m,k}, \tag{37a}$$

$$\bar{\mathbf{W}}_{l,i} = \bar{\mathbf{w}}_{l,i}\bar{\mathbf{w}}_{l,i}^H, \tag{37b}$$

$$\bar{\mathbf{R}}_l^r = \sum_{i \in \mathcal{K}_l} \mathbf{W}_{l,i}^{**} + \mathbf{R}_l^{r**} - \sum_{i \in \mathcal{K}_l} \bar{\mathbf{W}}_{l,i} \tag{37c}$$

$$\bar{\Omega} = \Omega^{**}. \tag{37d}$$

proof 2: The proof is similar to that in Appendix A, for which the details are omitted.

B. Scenario II without BSs Synchronization

Next, we consider Scenario II without BSs synchronization. In this scenario, the SINR-constrained minimum detection probability maximization problems of Type-I and Type-II CU receivers are respectively formulated as problems (P3) and (P4) in the following, which are similar to problems (P1) and (P2) by replacing $\mathcal{E}_{\text{I}}$ in (27) as $\mathcal{E}_{\text{II}}$ in (28), respectively:

$$(\text{P3}): \max_{\{\mathbf{w}_{m,i}, \mathbf{R}_m^r \succeq \mathbf{0}\}} \min_{q \in \mathcal{Q}} f^{\text{II}}\left(\{\mathbf{w}_{m,i}\}, \{\mathbf{R}_m^r\}\right) \tag{38}$$

$$\text{s.t.} \quad (30b) \text{ and } (30c).$$

$$(\text{P4}) : \max_{\{\mathbf{w}_{m,i}, \mathbf{R}_m^r \succeq \mathbf{0}\}} \min_{q \in \mathcal{Q}} f^{\text{II}} (\{\mathbf{w}_{m,i}\}, \{\mathbf{R}_m^r\}) \qquad (39)$$

$$\text{s.t. } (30c) \text{ and } (31b).$$

where

$$f^{\text{II}} (\{\mathbf{w}_{m,i}\}, \{\mathbf{R}_m^r\}) = \sum_{m \in \mathcal{L}} \zeta_{m,m}^2 \beta_{m,m}^{(q)} \text{tr}((\sum_{i \in \mathcal{K}_m} \mathbf{w}_{m,i} \mathbf{w}_{m,i}^H$$
$$+ \mathbf{R}_m^r) \mathbf{A}_m(\theta_m^{(q)})). \qquad (40)$$

As problems (P3) and (P4) have similar structures as problems (P1) and (P2), respectively, they can also be solved optimally based on the SDR. More specifically, by introducing the auxiliary variable Ω, and defining $\mathbf{W}_{m,i} = \mathbf{w}_{m,i} \mathbf{w}_{m,i}^H \succeq \mathbf{0}$ with $\text{rank}(\mathbf{W}_{m,i}) \leq 1$, problems (P3.1) and (P4.1) can be reformulated equivalently as

$$(\text{P3.1}) : \max_{\{\mathbf{W}_{m,i} \succeq \mathbf{0}, \mathbf{R}_m^r \succeq \mathbf{0}, \Omega\}} \Omega \qquad (41a)$$

$$\text{s.t. } \hat{f}^{\text{II}} (\{\mathbf{W}_{m,i}\}, \{\mathbf{R}_m^r\}) \geq \Omega, \forall q \in \mathcal{Q}, \qquad (41b)$$

$$(33c), (33d), \text{ and } (33e),$$

and

$$(\text{P4.1}) : \max_{\{\mathbf{W}_{m,i} \succeq \mathbf{0}, \mathbf{R}_m^r \succeq \mathbf{0}, \Omega\}} \Omega \qquad (42a)$$

$$\text{s.t. } (41b), (34b), (33d), \text{ and } (33e),$$

respectively, where

$$\hat{f}^{\text{II}} (\{\mathbf{W}_{m,i}\}, \{\mathbf{R}_m^r\}) = \sum_{m \in \mathcal{L}} \zeta_{m,m}^2 \beta_{m,m}^{(q)} \text{tr}((\sum_{i \in \mathcal{K}_m} \mathbf{W}_{m,i}$$
$$+ \mathbf{R}_m^r) \mathbf{A}_m(\theta_m^{(q)})) \qquad (43)$$

Then, we drop the rank-one constraints on $\{\mathbf{W}_{m,i}\}$ in (33e) to obtain the SDR versions of (P3.1) and (P4.1) as (SDR3.1) and (SDR4.1), respectively, which are convex and can be solved optimally.

Note that problems (SDR3.1) and (SDR4.1) generally have high rank optimal solutions, which may not satisfy the rank-one constraints in (33e) for (P3.1) and (P4.1). Fortunately, by following the similar concepts as in *Propositions 1* and *Propositions 2* for the SDRs of (P3.1) and (P4.1), one can show that the optimal rank-one solutions to (P3.1) and (P4.1) can always be constructed. The details of the derivations are thus omitted for brevity.

Remark 1: Comparing problem (P1.1) (or (P2.1)) in Scenario I with problem (P3.1) (or (P4.1)) in Scenario II, we observe that the feasible solutions of (P1.1) (or (P3.1)) is a subset of (P2.1) (or (P4.1)), but not vice versa. Thus, we conclude that problem (P2.1) (or (P4.1)) can always achieve a higher optimal objective value or at least equal to that of (P1.1) (or (P3.1)), since (P2.1) and (P4.1) enjoy a larger feasible solution set than (P1.1) and (P3.1), respectively. Moreover, via extensive simulations in the next section, we observe that for Type-I receivers without sensing signal interference cancellation, the optimal solutions to (P2.1) and (P4.1) satisfy $\mathbf{R}_l^r = \mathbf{0}$, which shows that employing dedicated sensing

signals is not necessary. Intuitively, this is because the dedicated sensing signals would introduce harmful interference for communications in this case.

V. NUMERICAL RESULTS

In this section, we provide numerical results to validate the performance of our proposed coordinated transmit beamforming designs for the multi-antenna networked ISAC system.

A. Benchmark Schemes

First, we consider the following benchmark schemes for performance comparison.

- **ISAC with ZF information beamforming**: In this scheme, we apply coordinated ZF beamforming [32], [45]. Let $\bar{\mathbf{H}}_{m,m,k} = [\mathbf{h}_{m,1,1}, \ldots, \mathbf{h}_{m,m,k-1}, \mathbf{h}_{m,m,k+1}, \ldots \mathbf{h}_{m,L,K}]$, and $\bar{\mathbf{H}}_{m,m,k} = \bar{\mathbf{U}}_{m,m,k} \bar{\mathbf{\Lambda}}_{m,m,k} \bar{\mathbf{V}}_{m,m,k}^H$ denotes the application of singular value decomposition (SVD) on $\bar{\mathbf{H}}_{m,m,k}$, where $\bar{\mathbf{U}}_{m,m,k} = [\bar{\mathbf{U}}_{m,m,k}^{\bar{\text{null}}} \bar{\mathbf{U}}_{m,m,k}^{\text{null}}]$ and $\bar{\mathbf{U}}_{m,m,k}^{\text{null}} \in \mathbb{C}^{N_t \times (N_t - L^2 K + 1)}$. The ZF transmit beamforming at BS m for CU k is designed as

$$\mathbf{w}_{m,k}^{\text{ZF}} = \frac{\sqrt{p_{m,k}^{\text{ZF}}} \bar{\mathbf{U}}_{m,m,k}^{\text{null}} \bar{\mathbf{U}}_{m,m,k}^{\text{null}H} \mathbf{h}_{m,m,k}}{\left\| \bar{\mathbf{U}}_{m,m,k}^{\text{null}} \bar{\mathbf{U}}_{m,m,k}^{\text{null}H} \mathbf{h}_{m,m,k} \right\|},$$
$$\forall m \in \mathcal{L}, \forall k \in \mathcal{K}_m, \qquad (44)$$

where $p_{m,k}^{\text{ZF}}$ denotes the power for CU k by BS m, which is a variable to be optimized. Accordingly, the power constraint at each BS m becomes $\sum_{k \in \mathcal{K}} p_{m,k}^{\text{ZF}} \leq P_{\max}$. By substituting $\mathbf{w}_{m,k}^{\text{ZF}}$ in (44) into problems (P1.1), (P2.1), (P3.1), and (P4.1), we obtain the corresponding power allocation problems (ZF1.1), (ZF2.1), (ZF3.1), and (ZF4.1), which can be optimized similarly as in Section IV for obtaining the optimal coordinated power control solutions.

- **Joint detection via dedicated sensing signals**: In this scheme, the BSs only employ the dedicated sensing signals for joint detection. The corresponding detection probabilities in Scenario I and Scenario II are respectively given by

$$p_{\text{D}}^{\text{I}} = Q \left(Q^{-1} \left(p_{\text{FA}}^{\text{I}} \right) - \sqrt{\frac{2 \hat{\mathcal{E}}_{\text{I}}}{\sigma_d^2}} \right), \qquad (45)$$

$$p_{\text{D}}^{\text{II}} = Q \left(Q^{-1} \left(p_{\text{FA}}^{\text{II}} \right) - \sqrt{\frac{2 \hat{\mathcal{E}}_{\text{II}}}{\sigma_d^2}} \right), \qquad (46)$$

where

$$\hat{\mathcal{E}}_{\text{I}} = N_r \sum_{l \in \mathcal{L}} \sum_{m \in \mathcal{L}} \zeta_{m,l}^2 \beta_{m,l} \text{tr}(\mathbf{R}_l^r \mathbf{A}_l(\theta_l^{(q)})), \qquad (47)$$

$$\hat{\mathcal{E}}_{\text{II}} = N_r \sum_{m \in \mathcal{L}} \zeta_{m,m}^2 \beta_{m,m} \text{tr}(\mathbf{R}_m^r \mathbf{A}_m(\theta_m^{(q)})), \qquad (48)$$

denote the correspondingly received echo signals of the dedicated sensing signals. Accordingly, we optimize the

joint beamforming by solving problems (P1)-(P4) via replacing $\mathcal{E}_{\mathrm{I}}$ and $\mathcal{E}_{\mathrm{II}}$ as $\hat{\mathcal{E}}_{\mathrm{I}}$ and $\hat{\mathcal{E}}_{\mathrm{II}}$, respectively.

B. Simulation Results

In the simulation, we consider the networked ISAC scenario with $L = 3$ BSs as shown in Fig. 2, where each BS serves one CU or multiple CUs. Each BS is deployed with a ULA with half a wavelength spacing between the antennas. The noise powers are set as $\sigma_c^2 = -84$ dBm and $\sigma_d^2 = -102$ dBm. The SINR constraints at the CUs are set to be identical, i.e., $\Gamma_{m,k} = \Gamma$, $\forall k \in \mathcal{K}_m, m \in \mathcal{L}$. The coordinates of the three BSs are set as $(80 \text{ m}, 0 \text{ m})$, $\left(-40 \text{ m}, 40\sqrt{3} \text{ m}\right)$, and $\left(-40 \text{ m}, -40\sqrt{3} \text{ m}\right)$, respectively. The numbers of transmit and receive antennas at each BSs are $N_t = N_r = N_a = 32$. Furthermore, the path loss between each BS and CU is given by $\mu_{l,i} = \hat{\kappa}[\frac{d_0}{d_{l,i}}]^\nu$, where $\hat{\kappa}$ denotes the path loss at the reference distance of $d_0 = 1$ meter and ν denotes the path loss exponent. In addition, the targeted area is set as a square region with an area of $2 \times 2 = 4$ m^2 centering at origin $(0 \text{ m}, 0 \text{ m})$, we take $M = 9$ sample locations that are uniformly distributed in the targeted area.
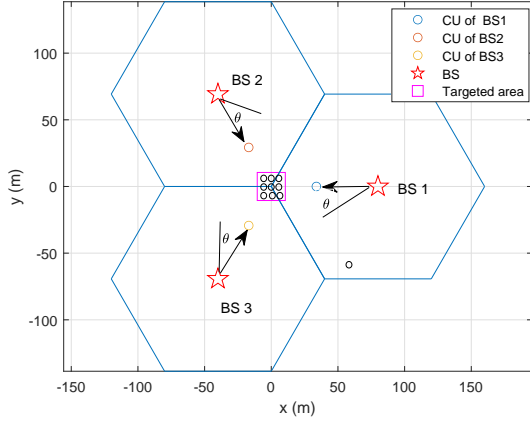
Fig. 2. The ISAC system has 3 BSs, each of which serves the corresponding CU for communication and detects the potential target at targeted area.

Firstly, we consider the case when there is only $K = 1$ CU served by each BS, thus the system has $LK = 3$ CUs in total. In particular, we consider the Rayleigh fading channel in communication from each BS to CU, and that the three CU locations are located at $(38.85 \text{ m}, -20.97 \text{ m})$, $(-1.26 \text{ m}, 44.13 \text{ m})$, and $(-37.58 \text{ m}, -23.16 \text{ m})$, respectively.

Fig. 3 shows the detection probability p_{D} versus the SINR requirement Γ at the CUs in Scenario I and Scenario II, in which the maximum transmit power constraint $P_{\max} = 15$W and the false alarm probability $p_{\mathrm{FA}} = 10^{-3}$. It is observed that for all the schemes, the detection probability decreases with an increasing SINR requirement. This is due to the fact that when the communication requirement becomes stringent, the BSs need to steer the transmit beamformers towards the CUs, thus leading to less power being reflected by the target location and jeopardizing the performance of detection. It is also observed that the proposed design with Type-II receivers achieves the highest detection probability compared to other
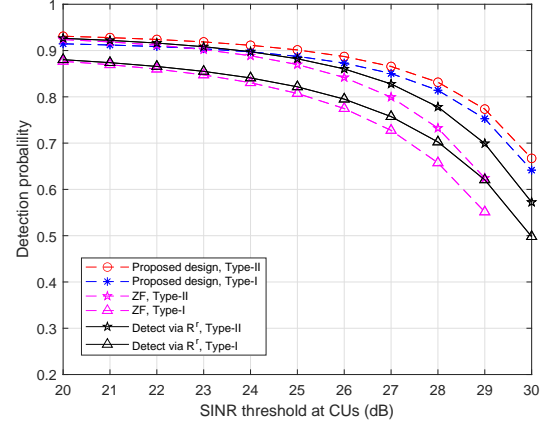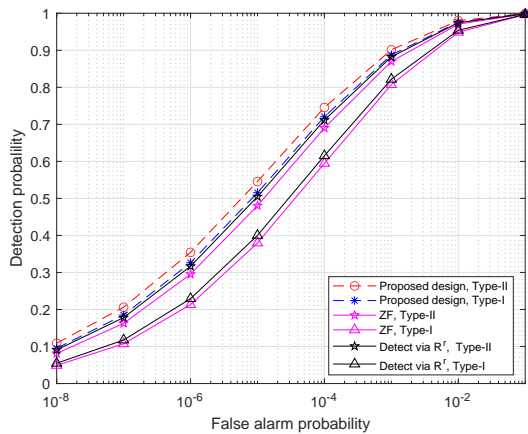
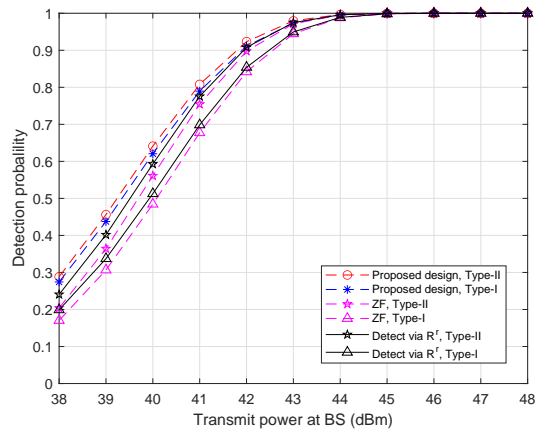

(a) Scenario I.
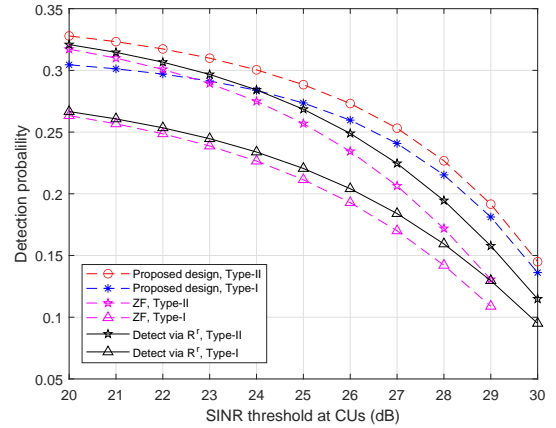
(b) Scenario II.

Fig. 3. The detection probability versus the SINR requirement at the CUs in Scenario I and Scenario II, where $P_{\max} = 15$ W, $K = 1$, and $p_{\mathrm{FA}} = 10^{-3}$.

schemes under same channel conditions in both Scenario I and Scenario II. When Γ becomes large, the performance gaps between the proposed design and the benchmark schemes are enlarged. This shows the importance of joint communication and sensing coordinated transmit beamforming. Furthermore, with a large value of Γ, the performance achieved by Type-I CU receivers approaches that of their Type-II counterparts. This is due to the fact that in this case, more power should be allocated to information signals. As a result, the power of dedicated sensing signals and the resultant interference become smaller, thus making the gain of sensing interference cancellation marginal.
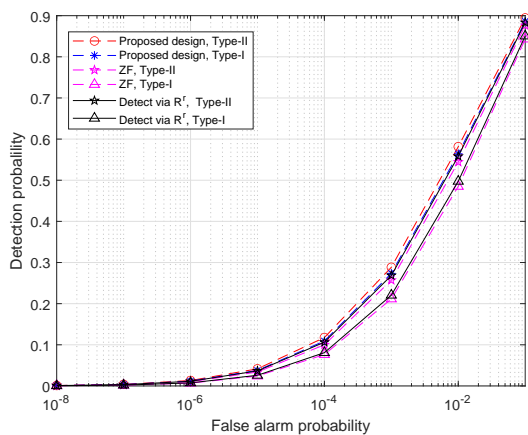
Fig. 4 shows the detection probability p_{D} versus the false alarm probability p_{FA} in the two scenarios for the two types of CU receivers with $P_{\max} = 15$ W and $\Gamma = 25$ dB. For all the schemes, it is observed that the detection probability increases towards one as the false alarm probability becomes large, as correctly predicted by (26) and (29). It is also observed that the detection probability achieved in Scenario II is much smaller than that in Scenario I under the same setup. This gain is attributed to the joint exploitation of both direct and cross echo links in Scenario I, thanks to the time synchronization among
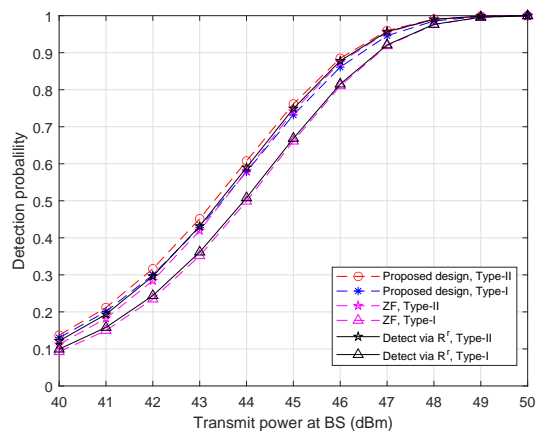
(a) Scenario I.

(a) Scenario I.

(b) Scenario II.

(b) Scenario II.

Fig. 4. The detection probability versus the false alarm probability in Scenario I and Scenario II, where $P_{\max} = 15$ W, $K = 1$, and $\Gamma = 25$ dB.

Fig. 5. The detection probability versus the transmit power at each BSs in Scenario I and Scenario II, where $\Gamma = 25$ dB, $K = 1$, and $p_{\text{FA}} = 10^{-3}$.

different BSs. Furthermore, the schemes with Type-II receivers are observed to achieve higher detection probability than the counterparts with Type-I receivers, thus validating again the benefit of dedicated sensing signals together with interference cancellation in enhancing the networked ISAC performance.

Fig. 5 shows the detection probability p_{D} versus the maximum transmit power budget $P_{\max}$ at each BS with $\Gamma = 25$ dB and $p_{\text{FA}} = 10^{-3}$. Similar observations can be made as in Figs. 3 and 4, demonstrating the performance gains achieved by the proposed joint optimization framework.

Next, we consider the case when each CU is located at a different angle with respect to its home BS, in which the LoS channel is considered in communication from each BS to its respective CU. In particular, as shown in Fig. 2, the CUs in different cells are located at the same angle θ with respect to the corresponding BS, and the distance between each BS and the correspondingly associated CU is 45 m.
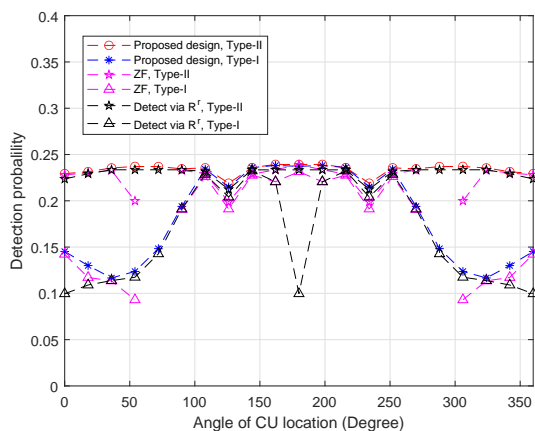
Fig. 6 shows the detection probability p_{D} versus the angle θ with $P_{\max} = 12$ W, $\Gamma = 30$ dB, and $p_{\text{FA}} = 10^{-3}$. It is observed that when θ is close to $0°$ and $360°$, the scheme with Type-II receivers significantly outperforms that with Type-I receivers. This is because the CUs are located at similar

angles as the targeted area in this case, and accordingly, the interference caused by sensing signals becomes severe. By contrast, when θ is close to $110°$, such performance gap is observed to become less. This is due to the fact that the CUs are located at different angles from the targeted area. As a result, the information and sensing beamformers can be steered toward different directions for communication and sensing, respectively, with minimized interference.

Furthermore, we consider that each BS serves $K = 3$ CUs, in which the Rayleigh fading channel model is considered from each BS to its respective CU. The locations of the CUs are generated as shown in Fig. 7. Fig. 8 shows the detection probability p_{D} versus the SINR requirement Γ at each CU, where $P_{\max} = 15$ W, $\Gamma = 15$ dB, $p_{\text{FA}} = 10^{-3}$. Fig. 9 shows the detection probability p_{D} versus the false alarm probability p_{FA} with $P_{\max} = 15$ W, $\Gamma = 15$ dB, and $p_{\text{FA}} = 10^{-3}$. Fig. 10 shows the detection probability p_{D} versus the power budget $P_{\max} = 15$ at each BS, with $\Gamma = 15$ dB, and $p_{\text{FA}} = 10^{-3}$. By comparing these figures to Figs. 3, 4, and 5 for the case with $K = 1$, it is observed that the proposed design with Type-I receivers achieves similar performance as that with Type-II receivers, which means that the gain brought by the
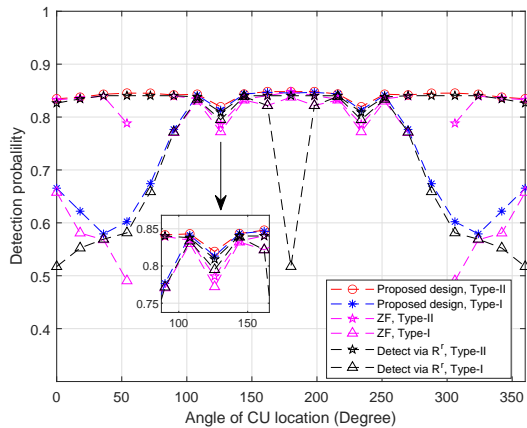
(a) Scenario I.

(b) Scenario II.

Fig. 6. The detection probability versus the angle θ at which the CU position has been rotated, where $P_{\max} = 12$ W, $\Gamma = 30$ dB, $K = 1$, and $p_{\mathrm{FA}} = 10^{-3}$.
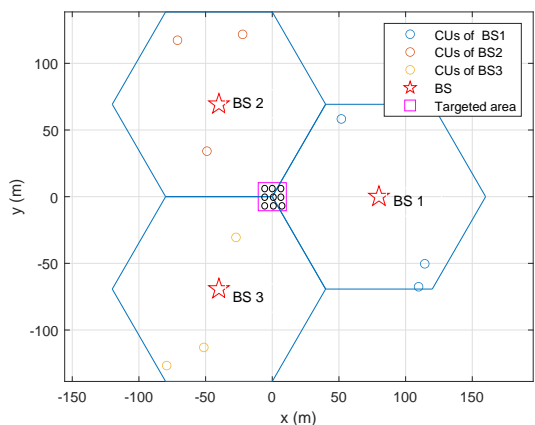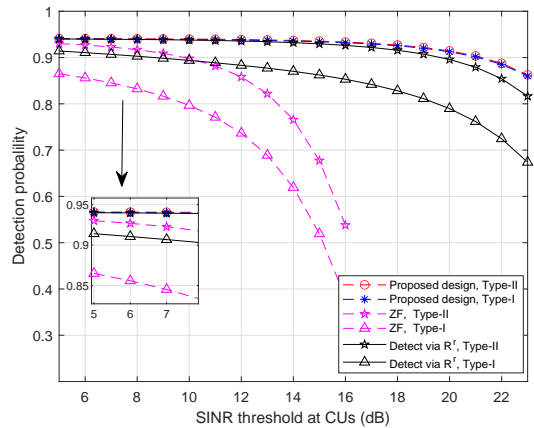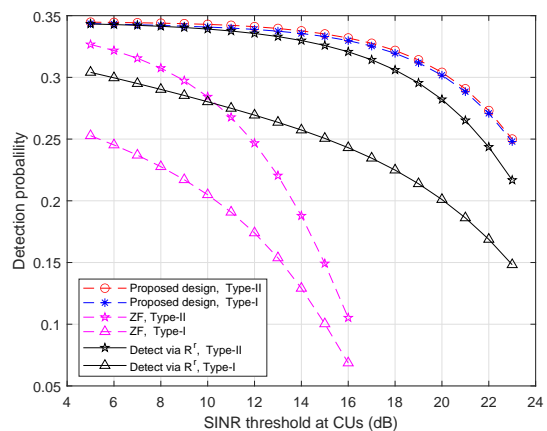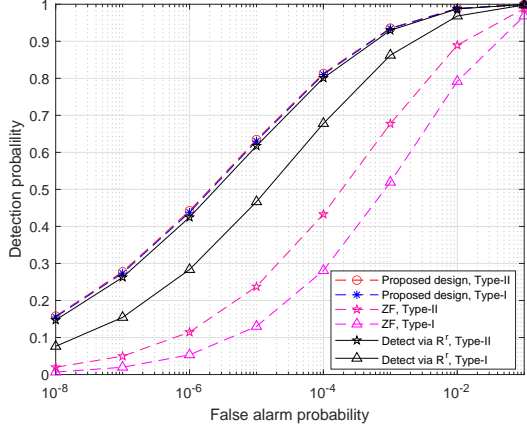

(a) Scenario I.

(b) Scenario II.

Fig. 8. The detection probability versus the SINR requirement at CUs in Scenario I and Scenario II, where $P_{\max} = 15$W, $\Gamma = 15$ dB, $K = 3$, and $p_{\mathrm{FA}} = 10^{-3}$.

Fig. 7. Networked ISAC topology with 3 BSs each serves 3 CUs (CU locations are randomly generated).

dedicated signals becomes marginal in this case. This is due to the fact that when there are more CUs in each cell, we have a larger number of information beams that can provide sufficient degrees of freedom for target sensing, thus making the benefit

of dedicated sensing signals limited or even not necessary. It is also observed that the benchmark scheme with ZF-based information beamforming performs significantly worse than the proposed designs. This is because with more CUs, the inter-user interference becomes more severe, and thus the ZF-based design leads to degraded performance due to the limited available degrees of freedom for effective interference suppression.

VI. CONCLUSION

This paper studied the joint multi-cell communication and distributed MIMO radar detection in a networked ISAC system, in which a set of multi-antenna BSs employed the coordinated transmit beamforming to serve their associated single-antenna CUs, and at the same time utilized the dedicated sensing signals together with their communication signals for target detection. Two joint detection scenarios with and without time synchronization among the BSs were considered, for which the detection probability and the false alarm probability were derived in closed forms. Accordingly, we developed the coordinated transmit beamforming ISAC design to maximize

(a) Scenario I.

(a) Scenario I.
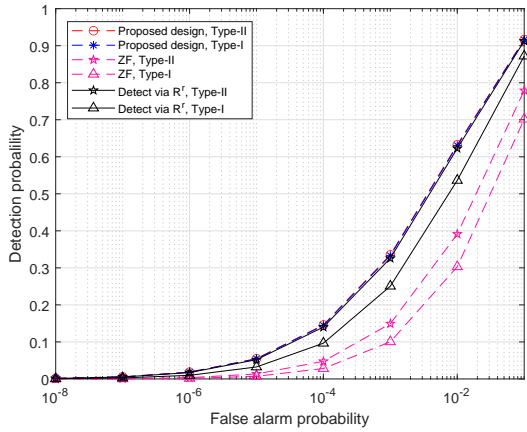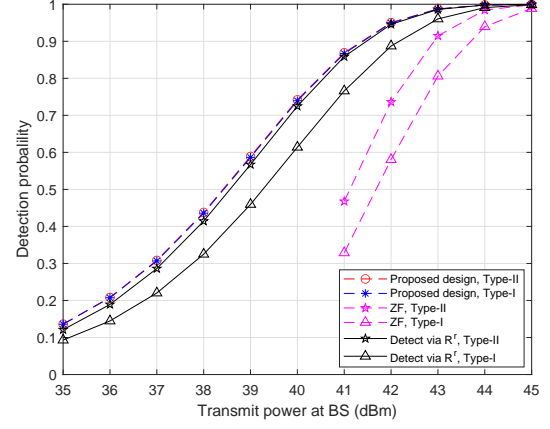

(b) Scenario II.

(b) Scenario II.

Fig. 9. The detection probability versus the false alarm probability in Scenario I and Scenario II, where $P_{\max} = 15$ W, $\Gamma = 15$ dB, $K = 3$, and $p_{\mathrm{FA}} = 10^{-3}$.

Fig. 10. The detection probability versus the transmit power in Scenario I and Scenario II, where $\Gamma = 15$ dB, $K = 3$, and $p_{\mathrm{FA}} = 10^{-3}$.

the minimum detection probability (or equivalently the total received reflection-signal power) over a particular targeted area, while ensuring the SINR constraints at the CUs for communication. By considering the transmission of dedicated sensing signals, we introduced two types of CU receivers, Type-I and Type-II, without and with the capability of dedicated sensing interference cancellation, respectively. For the proposed non-convex optimization problems, we adopted the SDR technique to obtain the optimal joint beamforming solutions. Finally, numerical results showed that the proposed ISAC design achieved higher detection probability than other benchmark schemes. It was also shown that the presence of time synchronization among the BSs and dedicated sensing interference cancellation can further enhance the sensing and communication performances for networked ISAC systems.
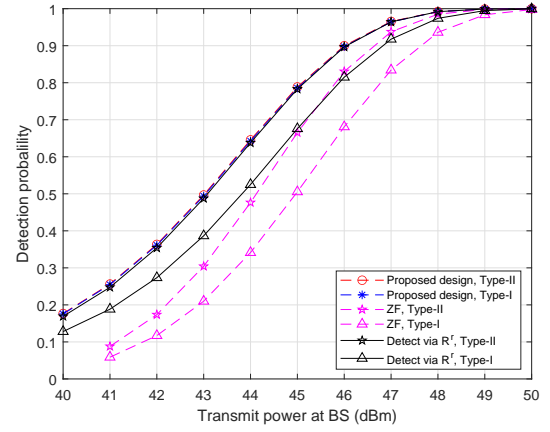
APPENDIX

A. Proof of Proposition 1

It can be verified based on (36a) and (36c) that $\tilde{\mathbf{W}}_{l,i}$ achieves the same objective values in (P1.1) as $\mathbf{W}_{l,i}^*$, and satisfy the power constraints in (33d).

Next, we verify that $\tilde{\mathbf{W}}_{l,i}$ can satisfy the SINR constraints in (33d) for communications. From (36a) and (36b), we obtain that

$$
\begin{aligned}
\mathbf{h}_{l,m,k}^H \tilde{\mathbf{W}}_{l,i} \mathbf{h}_{l,m,k} &= \mathbf{h}_{l,m,k}^H \tilde{\mathbf{w}}_{l,i} \tilde{\mathbf{w}}_{l,i}^H \mathbf{h}_{l,m,k} \\
&= \mathbf{h}_{l,m,k}^H \mathbf{W}_{l,i}^* \mathbf{h}_{l,m,k}.
\end{aligned} \tag{49}
$$

Thus, it follows that

$$
\begin{aligned}
&(1 + \frac{1}{\Gamma_{m,k}}) \mathbf{h}_{m,m,k}^H \tilde{\mathbf{W}}_{m,k} \mathbf{h}_{m,m,k} \\
&= (1 + \frac{1}{\Gamma_{m,k}}) \mathbf{h}_{m,m,k}^H \mathbf{W}_{m,k}^* \mathbf{h}_{m,m,k} \\
&\geq \sum_{l \in \mathcal{L}} \mathbf{h}_{l,m,k}^H (\sum_{i \in \mathcal{K}_l} \mathbf{W}_{l,i}^* + \mathbf{R}_l^{r*}) \mathbf{h}_{l,m,k} + \sigma_c^2 \\
&= \sum_{l \in \mathcal{L}} \mathbf{h}_{l,m,k}^H (\sum_{i \in \mathcal{K}_l} \tilde{\mathbf{W}}_{l,i} + \tilde{\mathbf{R}}_l^{r}) \mathbf{h}_{l,m,k} + \sigma_c^2.
\end{aligned} \tag{50}
$$

The first equality follows from (49), the inequality follows from (33c), and the last equality follows from (36c). Therefore, we show that the constructed solution $\{\tilde{\mathbf{W}}_{l,i}\}$ and $\{\tilde{\mathbf{R}}_l^{r}\}$ also satisfy the SINR constraints in (33d) for problem (P1.1). Thus, this completes the proof of this proposition.

References

[1] G. Cheng and J. Xu, "Coordinated transmit beamforming for multi-antenna network integrated sensing and communication," in *Proc. IEEE Int. Conf. Commun. (ICC)*, Rome, Italy, May 2023.

[2] F. Liu, C. Masouros, A. P. Petropulu, H. Griffiths, and L. Hanzo, "Joint radar and communication design: Applications, state-of-the-art, and the road ahead," *IEEE Trans. Commun.*, vol. 68, no. 6, pp. 3834–3862, Jun. 2020.

[3] F. Dong, F. Liu, Y. Cui, W. Wang, K. Han, and Z. Wang, "Sensing as a service in 6G perceptive networks: A unified framework for ISAC resource allocation," *IEEE Trans. Wireless Commun.*, vol. 22, no. 5, pp. 3522–3536, May 2023.

[4] Z. Wei, F. Liu, C. Masouros, N. Su, and A. P. Petropulu, "Toward multi-functional 6G wireless networks: Integrating sensing, communication, and security," *IEEE Commun. Mag.*, vol. 60, no. 4, pp. 65–71, Apr. 2022.

[5] X. Mu, Z. Wang, and Y. Liu, "NOMA for integrating sensing and communications towards 6G: A multiple access perspective," *IEEE Wireless Commun.*, pp. 1–8, early access, Jan. 2023, doi: 10.1109/MWC.015.2200559.

[6] F. Liu, Y. Cui, C. Masouros, J. Xu, T. X. Han, Y. C. Eldar, and S. Buzzi, "Integrated sensing and communications: Toward dual-functional wireless networks for 6G and beyond," *IEEE J. Sel. Areas in Commun.*, vol. 40, no. 6, pp. 1728–1767, Mar. 2022.

[7] K. Meng, Q. Wu, J. Xu, W. Chen, Z. Feng, R. Schober, and A. L. Swindlehurst, "UAV-enabled integrated sensing and communication: Opportunities and challenges," *IEEE Wireless Commun.*, pp. 1–9, early access, Apr. 2023, doi: 10.1109/MWC.131.2200442.

[8] M. Mozaffari, X. Lin, and S. Hayes, "Toward 6G with connected sky: UAVs and beyond," *IEEE Commun. Mag.*, vol. 59, no. 12, pp. 74–80, Dec. 2021.

[9] Z. Lyu, G. Zhu, and J. Xu, "Joint maneuver and beamforming design for UAV-enabled integrated sensing and communication," *IEEE Trans. Wireless Commun.*, vol. 22, no. 4, pp. 2424–2440, Oct. 2023.

[10] Z. Wang, Y. Liu, X. Mu, Z. Ding, and O. A. Dobre, "NOMA empowered integrated sensing and communication," *IEEE Commun. Lett.*, vol. 26, no. 3, pp. 677–681, Jan. 2022.

[11] H. Zhang, H. Zhang, B. Di, M. D. Renzo, Z. Han, H. V. Poor, and L. Song, "Holographic integrated sensing and communication," *IEEE J. Sel. Areas Commun.*, vol. 40, no. 7, pp. 2114–2130, Mar. 2022.

[12] F. Liu, C. Masouros, A. Li, and T. Ratnarajah, "Robust MIMO beamforming for cellular and radar coexistence," *IEEE Wireless Commun. Lett.*, vol. 6, no. 3, pp. 374–377, Jun. 2017.

[13] F. Liu, C. Masouros, A. Li, T. Ratnarajah, and J. Zhou, "MIMO radar and cellular coexistence: A power-efficient approach enabled by interference exploitation," *IEEE Trans. Signal. Process.*, vol. 66, no. 14, pp. 3681–3695, Jul. 2018.

[14] A. Khawar, A. Abdelhadi, and C. Clancy, "Target detection performance of spectrum sharing MIMO radars," *IEEE Sensors J.*, vol. 15, no. 9, pp. 4928–4940, Sep. 2015.

[15] P. Kumari, S. A. Vorobyov, and R. W. Heath, "Adaptive virtual waveform design for millimeter-wave joint communication-radar," *IEEE Trans. Signal Process.*, vol. 68, pp. 715–730, Nov. 2019.

[16] H. Hua, J. Xu, and T. X. Han, "Optimal transmit beamforming for integrated sensing and communication," *IEEE Trans. Veh. Technol.*, pp. 1–16, early access, Mar. 2023, doi: 10.1109/TVT.2023.3262513.

[17] F. Liu, C. Masouros, A. Li, H. Sun, and L. Hanzo, "MU-MIMO communications with MIMO radar: From co-existence to joint transmission," *IEEE Trans. Wireless Commun.*, vol. 17, no. 4, pp. 2755–2770, Feb. 2018.

[18] Z. Xiao and Y. Zeng, "Waveform design and performance analysis for full-duplex integrated sensing and communication," *IEEE J. Sel. Areas Commun.*, vol. 40, no. 6, pp. 1823–1837, Mar. 2022.

[19] X. Liu, T. Huang, N. Shlezinger, Y. Liu, J. Zhou, and Y. C. Eldar, "Joint transmit beamforming for multiuser MIMO communications and MIMO radar," *IEEE Trans. Signal Process.*, vol. 68, pp. 3929–3944, Jun. 2020.

[20] F. Liu, L. Zhou, C. Masouros, A. Li, W. Luo, and A. Petropulu, "Toward dual-functional radar-communication systems: Optimal waveform design," *IEEE Trans. Signal Process.*, vol. 66, no. 16, pp. 4264–4279, Jun. 2018.

[21] C. Xu, B. Clerckx, S. Chen, Y. Mao, and J. Zhang, "Rate-splitting multiple access for multi-antenna joint radar and communications," *IEEE J. Sel. Top. Signal Process.*, vol. 15, no. 6, pp. 1332–1347, Sep. 2021.

[22] D. Gesbert, S. Hanly, H. Huang, S. Shamai Shitz, O. Simeone, and W. Yu, "Multi-cell MIMO cooperative networks: A new look at interference," *IEEE J. Sel. Areas Commun.*, vol. 28, no. 9, pp. 1380–1408, Dec. 2010.

[23] H. Dahrouj and W. Yu, "Coordinated beamforming for the multicell multi-antenna wireless system," *IEEE Trans. Wireless Commun.*, vol. 9, no. 5, pp. 1748–1759, May 2010.

[24] J. Wu, Z. Zhang, Y. Hong, and Y. Wen, "Cloud radio access network (C-RAN): a primer," *IEEE Network*, vol. 29, no. 1, pp. 35–41, Jan. 2015.

[25] H. Q. Ngo, A. Ashikhmin, H. Yang, E. G. Larsson, and T. L. Marzetta, "Cell-free massive MIMO versus small cells," *IEEE Trans. Wireless Commun.*, vol. 16, no. 3, pp. 1834–1850, Jan. 2017.

[26] E. Fishler, A. Haimovich, R. Blum, D. Chizhik, L. Cimini, and R. Valenzuela, "MIMO radar: An idea whose time has come," in *Proc. IEEE Radar Conf.*, Aug. 2004, pp. 71–78.

[27] F. Daum and J. Huang, "MIMO radar: Snake oil or good idea?" *IEEE Aerosp. Electron. Syst. Mag.*, vol. 24, no. 5, pp. 8–12, May 2009.

[28] L. Xu, J. Li, and P. Stoica, "Target detection and parameter estimation for MIMO radar systems," *IEEE Trans. Aerosp. Electron. Syst.*, vol. 44, no. 3, pp. 927–939, Jul. 2008.

[29] A. M. Haimovich, R. S. Blum, and L. J. Cimini, "MIMO radar with widely separated antennas," *IEEE Signal Process. Mag.*, vol. 25, no. 1, pp. 116–129, Jan. 2008.

[30] Q. Shi, L. Liu, S. Zhang, and S. Cui, "Device-free sensing in OFDM cellular network," *IEEE J. Sel. Areas Commun.*, vol. 40, no. 6, pp. 1838–1853, Jun. 2022.

[31] Y. Huang, Y. Fang, X. Li, and J. Xu, "Coordinated power control for network integrated sensing and communication," *IEEE Trans. Veh. Technol.*, vol. 71, no. 12, pp. 13 361–13 365, Mar. 2022.

[32] Z. Behdad, Ö. T. Demir, K. W. Sung, E. Björnson, and C. Cavdar, "Power allocation for joint communication and sensing in cell-free massive MIMO," in *Proc. 2022 IEEE Global Commun. Conf. (GLOBECOM)*, Dec. 2022, pp. 4081–4086.

[33] X. Wang, Z. Fei, J. A. Zhang, J. Huang, and J. Yuan, "Constrained utility maximization in dual-functional radar-communication multi-UAV networks," *IEEE Trans. Commun.*, vol. 69, no. 4, pp. 2660–2672, Apr. 2021.

[34] M. L. Rahman, J. A. Zhang, X. Huang, Y. J. Guo, and R. W. Heath, "Framework for a perceptive mobile network using joint communication and radar sensing," *IEEE Trans. Aerosp. Electron. Syst.*, vol. 56, no. 3, pp. 1926–1941, Sep. 2019.

[35] A. Zhang, M. L. Rahman, X. Huang, Y. J. Guo, S. Chen, and R. W. Heath, "Perceptive mobile networks: Cellular networks with radio vision via joint communication and radar sensing," *IEEE Veh. Technol. Mag.*, vol. 16, no. 2, pp. 20–30, Jun. 2021.

[36] Z. Ni, J. A. Zhang, X. Huang, K. Yang, and J. Yuan, "Uplink sensing in perceptive mobile networks with asynchronous transceivers," *IEEE Trans. Signal Process.*, vol. 69, pp. 1287–1300, Feb. 2021.

[37] L. Xie, S. Song, Y. C. Eldar, and K. B. Letaief, "Collaborative sensing in perceptive mobile networks: Opportunities and challenges," *IEEE Wireless Commun.*, vol. 30, no. 1, pp. 16–23, Feb. 2023.

[38] E. Fishler, A. Haimovich, R. Blum, L. Cimini, D. Chizhik, and R. Valenzuela, "Spatial diversity in radars - models and detection performance," *IEEE Trans. Signal Process.*, vol. 54, no. 3, pp. 823–838, Mar. 2006.

[39] N. H. Lehmann, A. M. Haimovich, R. S. Blum, and L. Cimini, "High resolution capabilities of MIMO radar," in *Proc. 40th Asilomar Conf. Signals, Syst. Comput.*, Nov. 2006, pp. 25–30.

[40] H. Godrich, A. M. Haimovich, and R. S. Blum, "Target localization accuracy gain in MIMO radar-based systems," *IEEE Trans. Inf. Theory*, vol. 56, no. 6, pp. 2783–2803, Jun. 2010.

[41] X. Song, T. X. Han, and J. Xu, "Cramér-Rao bound minimization for IRS-enabled multiuser integrated sensing and communication with extended target," in *Proc. IEEE Int. Conf. Commun. (ICC)*, Rome, Italy, May 2023.

[42] S. M. Kay, *Fundamentals of Statistical Signal Processing: Estimation Theory*. Cliffs, NJ, USA: Prentice-Hall, 1993.

[43] Z. Luo, W. Ma, A. M. So, Y. Ye, and S. Zhang, "Semidefinite relaxation of quadratic optimization problems," *IEEE Signal Process. Mag.*, vol. 27, no. 3, pp. 20–34, May 2010.

[44] M. Grant and S. Boyd, "CVX: Matlab software for disciplined convex programming, version 2.1," 2014. [Online]. Available: http://cvxr.com/cvx/

[45] R. W. Heath Jr and A. Lozano, *Foundations of MIMO communication*. 1st ed. Cambridge, U.K.: Cambridge Univ. Press, Dec. 2018.